Energy dissipation and transfer processes during the breaking of modulated wave trains

2015 J. Phys.: Conf. Ser. 655 012037

(http://iopscience.iop.org/1742-6596/655/1/012037)

Journal of Physics: Conference Series **655** (2015) 012037 doi:10.1088/1742-6596/655/1/012037

Energy dissipation and transfer processes during the breaking of modulated wave trains

F De Vita[1,2], R Verzicco[1] and A Iafrati[2]

[1] University of Rome "Tor Vergata", 1 Politecnico street, 00133 Rome, Italy
[2] CNR-INSEAN Marine Technology Research Institute, 139 Vallerano street, 00128 Rome, Italy

E-mail: Francesco.De.Vita@uniroma2.it

Abstract. In this work numerical simulation of the breaking induced by the modulational instability are presented. The study is focused on the energy and momentum exchanged taking place at the air-water interface during the breaking process. Simulations are performed by a two-fluids Navier-Stokes solver combined with the VOF technique, which provides a detailed description of the flow in both phases. Results obtained by two different initial conditions are presented in terms of free surface shapes, energy in air and water, vertical fluxes of horizontal momentum and vorticity.

1. Introduction

In fully developed sea, ocean and atmosphere are strongly coupled, exchanging mass, momentum and heat through their interface. The ocean waves themselves are the most evident result of the interaction and of the energy input from wind to the wave system [1]. However, even if perhaps less intuitive, there is evidence that the ocean surface cannot be regarded as a flat and passive surface when modelling the wind blowing on top of it [2] and thus the coupled system should be considered for reliable weather and climate forecasting [3].

There are several phenomena taking place at the interface, but the one which is by far the most relevant for the exchange processes at the interface is the wave breaking. The breaking is a strongly nonlinear phenomenon which occurs when the wave grows too much and exceeds some limiting conditions. There are two main mechanisms which make it to happen, which are the linear superposition and the modulational instability, the latter being much more frequent [4]. Regardless the way which leads to its development, the wave breaking occurrence injects horizontal momentum and leads to a strong mixing of the upper ocean layer, with the entrainment of air bubbles [5] and the release of sea droplets which affect the atmospheric boundary layer [6].

Despite its important role, the physics of the breaking phenomenon is not well understood and many points are still obscure. As highlighted in [7], breaking models currently adopted for the breaking in wave forecasting are strongly dependent on their parameters and changing them makes the predictions more or less in agreement with the recorded data.

The development of accurate breaking models is hindered by the difficulties of realizing field measurements, but even in laboratory the situation is not much better. In spite of many detailed experiments which have been performed, there are technical limitations which make it rather difficult

to perform detailed non-intrusive investigation of the two-phase flow. For instance, due to the light reflection from the air-water interface, the use of optical measurement techniques is allowed only in a later stage when the largest air bubbles have degassed [8], and thus there are no information for the early stage of the breaking process which is when the most relevant exchange processes take place. Due to the lack of detailed data on the velocity field, the wave energy is computed on the basis of the free surface elevation only [9], thus neglecting the energy amount associated to the rotational flow generated by the breaking process and leading to incorrect estimates of the energy losses. Last but not least, only a little is known for the flow above the free surface and for the air water interaction.

All the above aspects can be investigated by highly detailed simulations of the two-phase flow. Although the numerical modelling is still very expensive from the computationally viewpoint, and thus sometime limited in the scales of the problems which can be faced, it provides a complete picture of the phenomenon and makes it possible to derive all the data which are needed for the analysis [10], [11]. Such models are used here to study the air-water interaction taking place during the breaking event with particular regard to the derivation of quantitative estimates of the exchange processes.

As a specific application, the breaking generated as a result of the modulational instability is here considered being representative of the open ocean conditions. The simulation is started from a fundamental component with sideband perturbations. Under suitable conditions [12], the modulational instability develops giving rise to a steep wave which breaks when a limiting steepness is exceeded [13]. The flow, both in air and water, is simulated by a Navier-Stokes solver for the multiphase system, which uses a Volume of Fluid technique for the interface capturing. Results are presented in term of energy transfer, vorticity generation and momentum flux. Comparisons of the solutions obtained when using different values of the initial steepness are also established.

2. Numerical Setup

The breaking of water waves induced by the classical Benjamin-Feir instability mechanism [14] is simulated numerically by a two-fluid method. The initial solution is composed by a fundamental wave component with two sideband perturbations. The free surface elevation $\eta(x,0)$ is initialized as:

$$\eta(x,0) = \frac{\varepsilon_0}{k_0}[\cos(k_0 x) + \alpha\cos(k^+ x) + \alpha\cos(k^- x)] \qquad 2.1$$

where $k_0 = 2\pi/\lambda_0$ and $\varepsilon_0 = k_0 A_0$ are the wavenumber and the initial steepness of the foundamental component, respectively, λ_0 and A_0 the corresponding wavelength and amplitude, α is the relative amplitude of the sideband perturbations and k^+ and k^- are the wavenumbers of the sideband ($k^+ = k_0 + \Delta k$ and $k^- = k_0 - \Delta k$).

In [13] it is shown that for $\alpha = 0.1$ and $\Delta k = k_0/5$ the breaking occurs when $\varepsilon_0 = 0.12$ and, with the increase of the initial steepness, it gets stronger and starts earlier. Most of the results of this work are presented for $\varepsilon_0 = 0.20$.

The velocity field in water is initialized from the linear theory as:

$$\begin{aligned} u(x,y,0) &= A_0\left[(gk_0)^{1/2}e^{(k_0 y)}\cos(k_0 x) + \alpha(gk^+)^{1/2}e^{(k^+ y)}\cos(k^+ x) + \alpha(gk^-)^{1/2}e^{(k^- y)}\cos(k^- x)\right] \\ v(x,y,0) &= A_0\left[(gk_0)^{1/2}e^{(k_0 y)}\sin(k_0 x) + \alpha(gk^+)^{1/2}e^{(k^+ y)}\sin(k^+ x) + \alpha(gk^-)^{1/2}e^{(k^+ y)}\sin(k^+ x)\right] \end{aligned} \qquad 2.2$$

where g is the gravity acceleration, which is 9.81 ms^{-1}.

Simulation are performed using the open-source Gerris software (http://gfs.sourceforge.net) which solves the incompressible Navier-Stokes equations and has a quad-octree discretization with adaptive mesh refinement. The solver is based on a projection method and use a multilevel Poisson solver (for more details see [15]). The multiphase flow is modelled using the one-fluid approach with the fluids properties depending on the variable $T(\boldsymbol{x},t)$ representing the volume fraction of the two fluid (*i.e.* the ratio between one fluid in the other so that $T = 1$ represents the air domain and $T = 0$ the water domain). The governing equations are the momentum equation:

$$\frac{d\boldsymbol{u}}{dt} = \frac{1}{\rho(T)}\{-\nabla p + \nabla \cdot [\mu(T)(\nabla \boldsymbol{u} + \nabla \boldsymbol{u}^T)] + \sigma k \delta_s \boldsymbol{n}\} \quad 2.3$$

for the fluid, and the advection equation for the volume fraction field:

$$\frac{\partial T}{\partial t} + \nabla \cdot (T\boldsymbol{u}) = 0 \quad 2.4$$

where $\boldsymbol{u}$ and p denote velocity and pressure, respectively, $\rho(T)$ and $\mu(T)$ the local fluid density and viscosity, k the interface curvature, σ the surface tension coefficient and δ_s the Dirac distribution which is zero out of the interface. The fluid properties are related to the variable T as:

$$\begin{aligned} \rho(T) &= \rho_a T + \rho_w(1-T) \\ \mu(T) &= \mu_a T + \mu_w(1-T) \end{aligned} \quad 2.5$$

The simulation are performed using the real parameters for air and water, which are:

$$\mu_w = 1.81\ 10^{-5}\ \text{Nsm}^{-2},\ \mu_a = 1.0\ 10^{-3}\ \text{Nsm}^{-2},\ \rho_a = 1.125\ \text{kg/m}^3,\ \rho_w = 1000\ \text{kg/m}^3,\ \sigma = 0.073\ \text{Nm}^{-1}$$

The wavelength of the foundamental component is λ_0 = 0.6 m, which is also the main scaling length, the domain width is $5\lambda_0$ and the height is $3\lambda_0$. Periodic boundary conditions are enforced at the right and left boundaries of the domain whereas free-slip boundary conditions are imposed at the top and the bottom boundaries.

The non-dimensional parameters characterizing this problem are the Reynolds and Weber numbers which are defined as:

$$\begin{aligned} Re &= \frac{\rho_w (g\lambda_0)^{1/2}\lambda_0}{\mu_w} = 1455664.8 \\ We &= \frac{\rho_w (g\lambda_0)^{1/2}\lambda_0}{\sigma_w} = 219.95 \end{aligned} \quad 2.6$$

where $(g\lambda_0)^{1/2}$ is the reference velocity, which is related to the phase velocity. It is worth noticing that the Reynolds number based on the phase velocity is not fully representative of the viscous phenomena taking place during the breaking process. A definition of the Reynolds number more representative of the physics should be based on the crest-to-trough velocity jump and on the wave height at the onset of the breaking. With such a definition, the Reynolds number would be approximatively 60000, which is two order of magnitude smaller than that based on the phase speed and makes simulations technically feasible. However, it is difficult to get a unique definition of those parameters as they strongly depend on the criteria adopted to define the onset of the breaking as well as on the points used to extract the velocities at crest and trough. In order to avoid such ambiguities, it was preferred to keep the definition based on the phase velocity despite its limitations.

Due to the high Re numbers, convergence analyses on the energy dissipation (not showed here) were made, and it was found that a maximum resolution of 2048 points per wavelength is enough to resolve the main dissipations scale of the phenomenon. This resolution is not enough to resolve all the dissipative scales but since the main contribution to the energy decay is due to the breaking, which involves larger scales of motion, allows to describe correctly the process. With such a resolution, the highest refinement level corresponds to a total of 10240 x 6144 grid cells. The use of the adaptive refinement capabilities allows to coarsen the grid outside the most relevant regions. The refinement level is based on vorticity and gradient of the interface function. With such choice, the grid about the free surface is always at the highest resolution level.

3. Results

During the evolution of the wave system the two sidebands grow whereas the foundamental component decreases due to nonlinear effects, as shown both experimentally in [12] and numerically in [13]. The growth of the sidebands leads to the formation of one wave in the group which is steeper than others. The steepness of the steepest wave, while increasing due to the nonlinear interaction, oscillates in time with a period which is twice the period of the fundamental component T, the maximum being achieved when the wave passes at the peak of the envelope. When the steepness exceeds a limiting value of 0.32, the breaking commences [16]. It last only a short fraction of the wave period as the modulational process causes a reduction of the steepness but then another breaking event occur in $2T$. In Fig. 1 the free surface profiles at different time instants are shown. The breaking starts with the formation of a bulge at the crest which slides down along the forward face, eventually leading to the entrainment of air cavities which are successively fragmented into smaller bubbles, the largest ones rising back towards the free surface and the finest remaining entrained in the vortical flow. The profiles display the formation of a second breaking event about $2T$ after the first event, which is in agreement with the field measurements in [17].

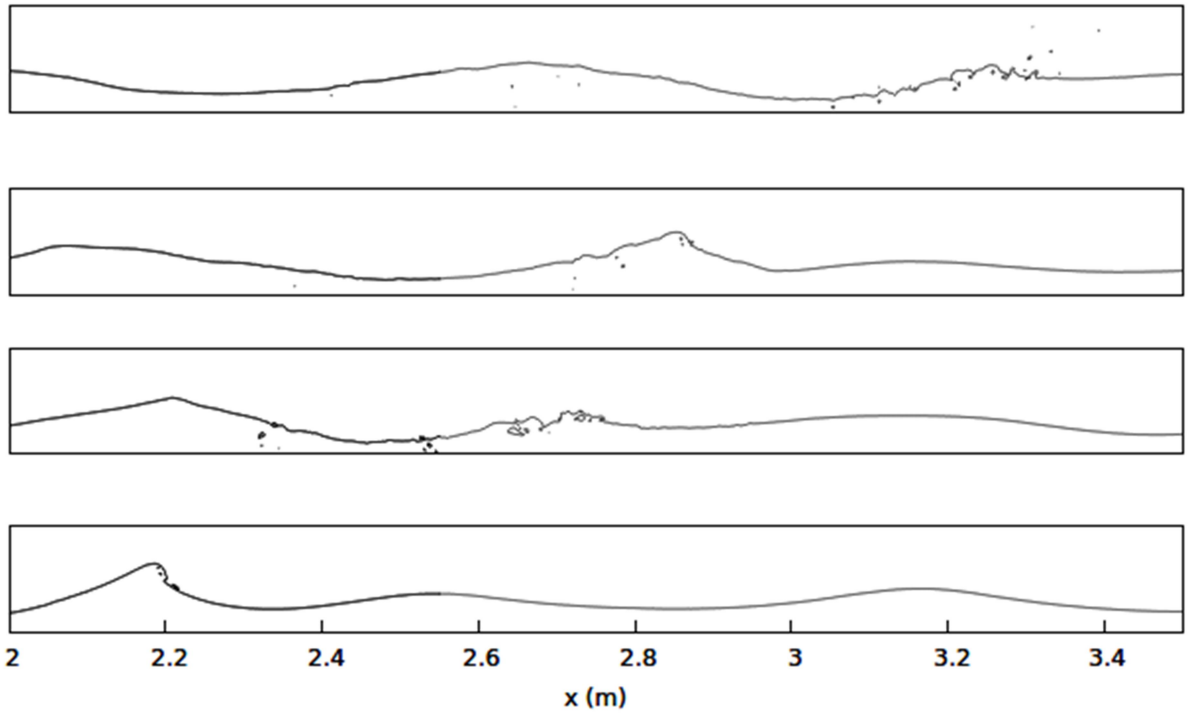

Figure 1. Surface elevation at different instant (the time grows from the bottom to the top) form $t = 14.5s$ to $t = 16\ s$. The time interval between two configuration is equal to the wave period, $T = 0.62\ s$. The wave is travelling from the left to right.

The important role played by the breaking on the exchange processes at the interface is clearly highlighted by the associated generation of bubbles and droplets. It is worth noting that, in spite of the quite high resolution adopted (the cell size is about 0.3 mm), not all scales are adequately resolved and, furthermore, phenomena like dissolution and aerosol or evaporation are not accounted for by the adopted model. Such phenomena provide significant contributions to the heat and gas transfer at the ocean-atmosphere interface. Due to the above mentioned limits, the results are focused on the analysis of the energy transfer and the vertical flux of horizontal momentum. The latter in particular helps in

estimating the thickness of the layer about the interface where advection processes are enhanced by the flow induced by the breaking.

3.1. Mechanical Energy

In order to evaluate the energy transfer between the two fluids, the total energy of water and air is computed as:

$$E_T(t) = \int_V (E_k + E_p) dV = \int_V \left(\rho g y + \frac{1}{2} \rho (u^2 + v^2) \right) dV - E_{p0} \qquad 3.1$$

where E_k is the kinetic energy, E_p is the potential energy and E_{p0} is the potential energy of the still water level. Figure 2 shows the time history of the total energy in air and water normalized with the initial energy content in water. The data refer to the case with initial steepness 0.20. In the early stage there is a rather mild energy reduction in water. This is because, before the onset of the breaking, the flow is essentially irrotational and viscous effects are rather weak [18]. When the breaking starts there is the formation of a plunging jet that impacts onto the free surface, leading to the formation of a rotational flow in water and to air entrainment. After the large air cavity is entrained it starts rotating and it is progressively squeezed and fragmented into small bubbles [5,10]. The bubble fragmentation process generates strong velocity gradients at small scales which significantly enhances the mixing and the dissipation process [10].

The breaking occurrence is also responsible for the transfer of energy to the air (right picture in figure 2). The energy transfer is operated by both tangential and normal stresses at the interface. Although the latter are expected to be dominant, a deeper investigation is needed to achieve a quantitative estimate of the two contributions.

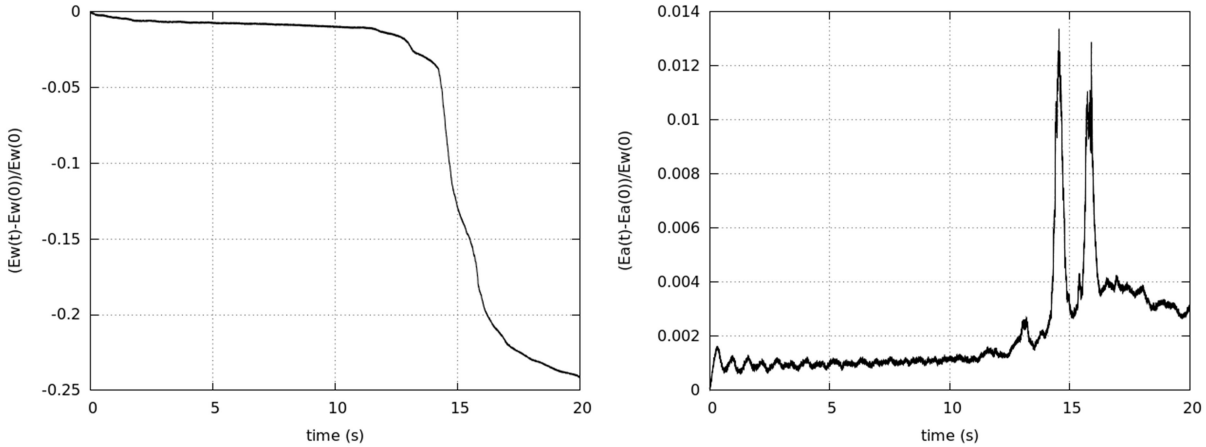

Figure 2. The figure shows the time history of the normalized energy for the case with initial steepness $\varepsilon_0 = 0.20$ in the water domain (left) and the air domain (right).

For the case considered in the present study, the total amount of energy lost by the water during the whole breaking process is about 25% of the initial energy content. For the same case, the energy amount accumulated in the air phase is about 1%. However, as discussed in [19], this is only a small fraction of the energy which is actually dissipated in the air. Indeed, due to the higher value of the kinematic viscosity and to the stronger velocity gradients, the dissipation rate in air is much higher than in water and most of the energy transferred in the air disappears before being accumulated.

As shown in figure 3, the results are essentially the same for the case with initial steepness 0.22. Due to the larger value of the initial steepness, the breaking starts somewhat earlier. The breaking events are more distinguished in this case but there are no significant differences in terms of the total energy fraction dissipated by the breaking and of the energy amount accumulated in air.

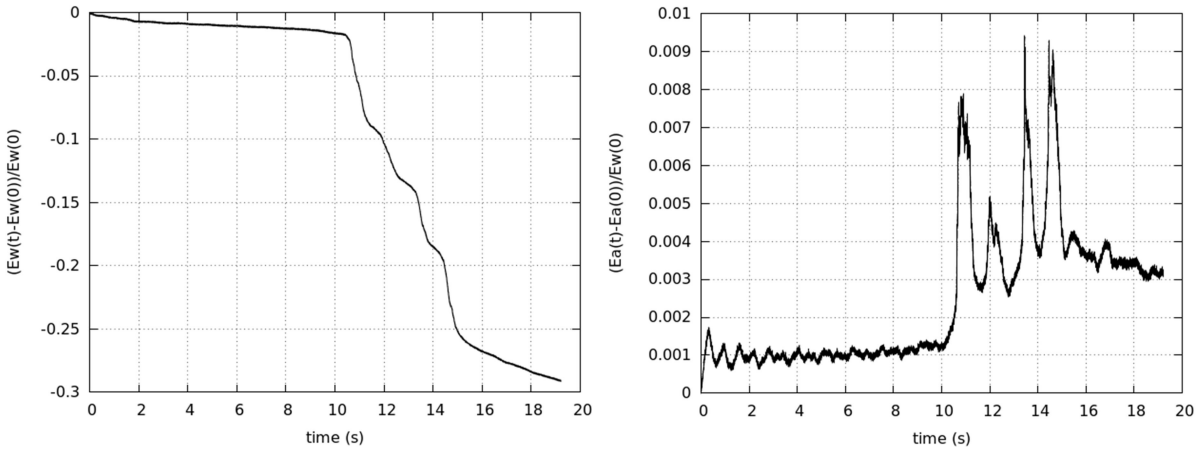

Figure 3. The figure shows the time history of the normalized energy for the case with initial steepness $\varepsilon_0 = 0.22$ in the water domain (left) and the air domain (right).

It is worth noting that, although the total amount is the same, the energy fraction dissipated by the single breaking events exhibits quite large variations from one event to the other, which explains the large scatter found in the experimental data [20].

3.2. Momentum transfer

In order to analyze the vertical transfer of the horizontal momentum, the flux:

$$q(y,t) = \int_x \rho u v \, dx \qquad 3.2.1$$

is computed along several horizontal lines, both in air and water, with a vertical distance of 0.005 m. Hence, the total amount of horizontal momentum transferred across each line at a given time τ is given by:

$$q(y,\tau) = \int_0^\tau q(y,t)dt \qquad 3.2.2$$

Figure 4 shows the total flux $q(y,\tau)$ transferred during the breaking process (i.e. from $t = 12$ *s,* which is when the breaking starts, up to $t = 16$ *s*). In order to avoid any misleading effect which could be caused by the crossing of the air-water interface through the lines, the fluxes are evaluated only for $y <$ -0.04 m and $y > 0.065$ m. Results indicate that the water layer affected by the momentum transfer is about 0.15 m thick, which is about one-fourth of the wavelength. Much deeper is the propagation of the momentum into the atmospheric layer, with some effects arriving up to one wavelength above the free surface. This has important consequences on the heat and gas transfer processes at the sea surface. It is worth noting that in this case the effects of the wind are missing. In a more realistic windy condition, it is expected that the interaction of the air flow induced by the breaking with the wind further enhances the exchange and transfer processes. The momentum flux is negative in water and positive in air meaning that there is a mean vertical current which is downward in water and upward in air.

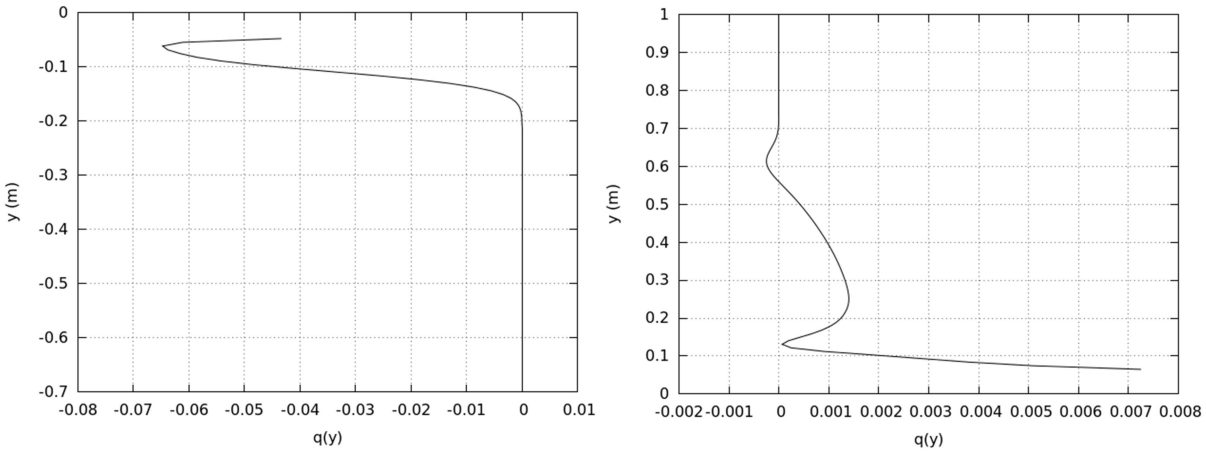

Figure 4. The figure shows the total horizontal momentum transferred in the y direction during the whole breaking process in the water domain (left) and in the air domain (right).

3.3. Vorticity

When the breaking starts, the wave develops a sharp curvature at the crest which induces the separation of the air flow. Due to the flow separation, the normal stresses at the interface at the front and at the rear of the wave crest are no longer balanced, and this contributes substantially to the energy and momentum transfer from the water to the air. Besides the normal stresses, tangential stresses are also quite strong. The flow separation gives rise to the development of a strong vorticity field in the air layer, and the periodicity of the flow associated to the orbital motion of the wave, leads to the shedding of large coherent structures [13].

Figure 5 shows the vorticity field at four different instants. As already indicated by the momentum transfer, the vorticity structures propagate much deeper into the air and some structures arrive even beyond one wavelength above the free surface. The sequence also highlights the vorticity generation in water. The structures in water are much smaller in size and, moreover, due to the lower velocities the downward motion is slower. Partly, such differences are due to the different viscosity value. But the higher velocities in air are also related to the momentum transfer at the interface in combination to the high density ratio of the two fluids.

Figure 6 shows a detailed view of the vorticity field both in water and in air. In the air, structures with different size appear, some of them being generated by the viscous effects at the free surface and others originated by the interaction with the sprays and droplets ejected in the breaking process (e.g. left picture in figure 7). In water, structures are generally much smaller. Also in this case some of them are generated by viscous effects at the interface, see [21], and others are generated by the air entrainment and by the fragmentation process. Aside from the generation mechanism, the vortex structures in water remain in an upper layer, just beneath the free surface.

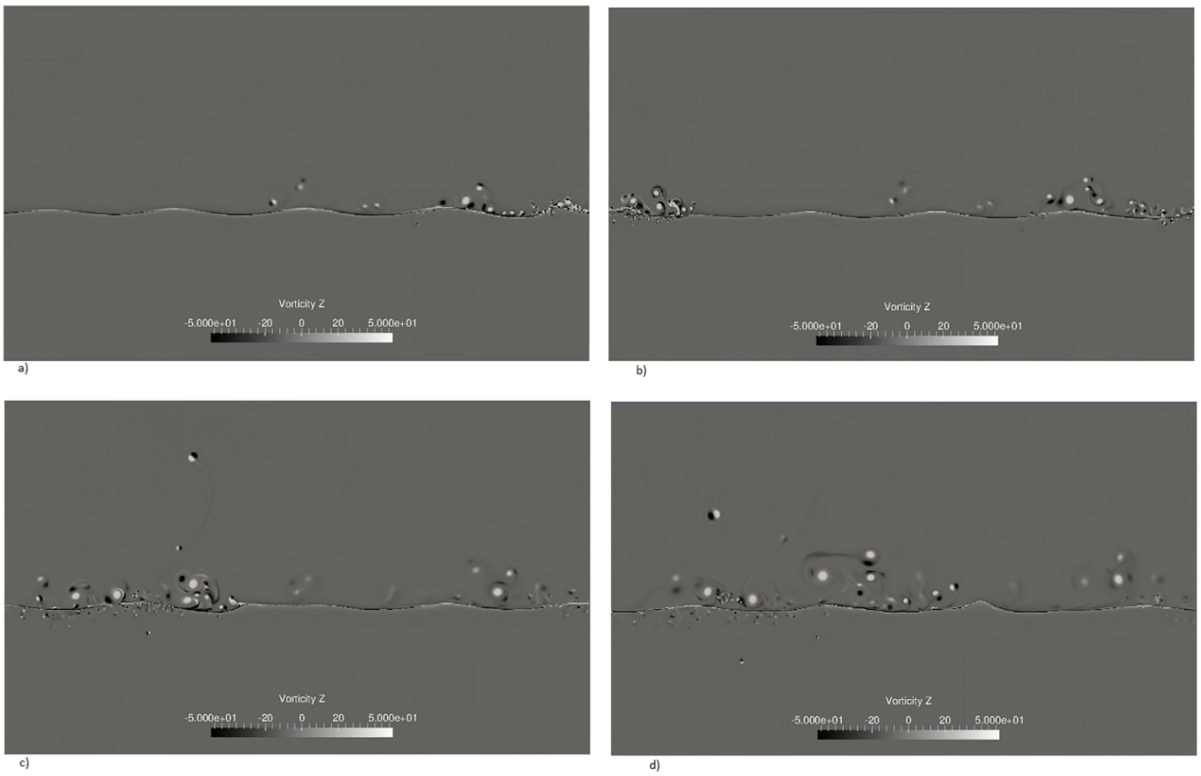

Figure 5. The figure shows the vorticity field distribution at four different instant: a) 14.55 s, b) 15.35 s, c) 17.20 s, d) 18.9 s**.**

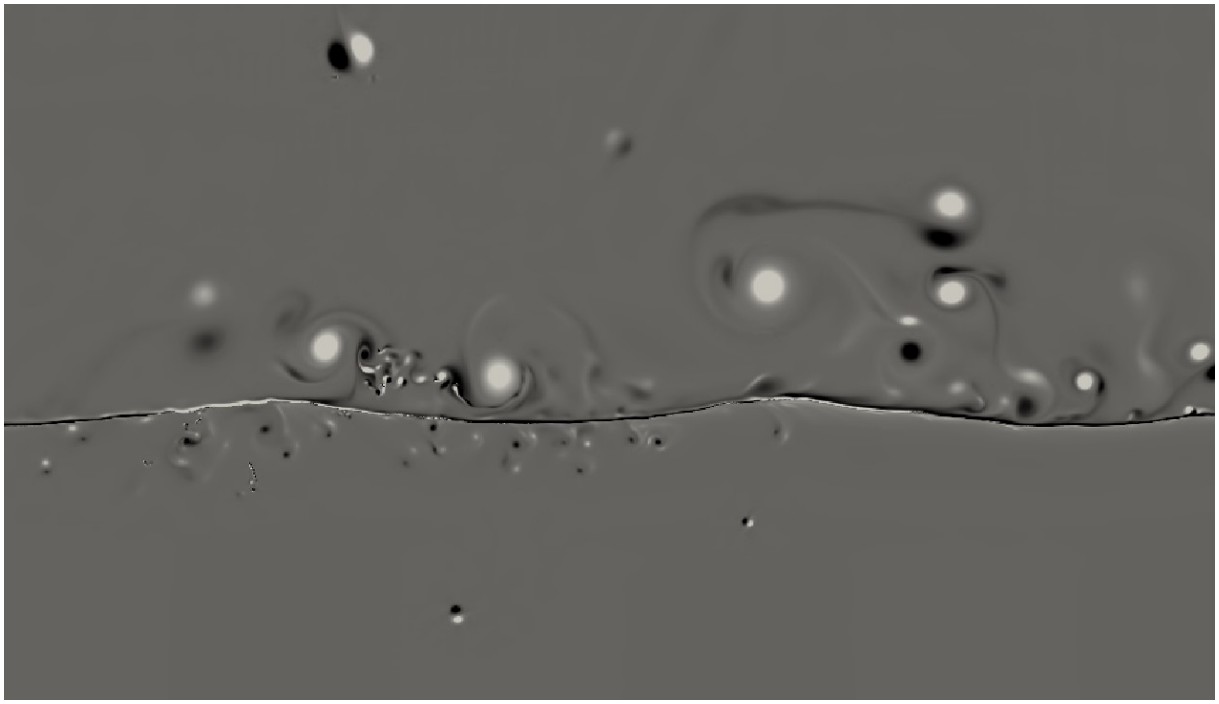

Figure 6: The figure shows a detail view of the vorticity field both in water and air at t = 18.90 s (the colours are the same of figure 5).

By increasing the initial steepness, the vorticity field is more intense both in air and water, the latter mainly related to the augmented level of air entrainment (figure 7).

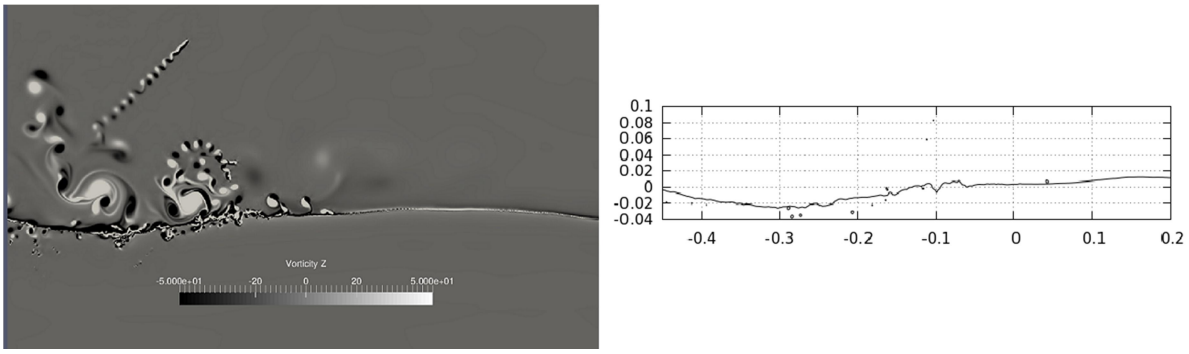

Figure 7. The figure shows a detailed view of the vorticity field for the case with initial steepness ε_0 = 0.22 both in the water domain (left) and in the air domain (right) at time t = 15 s. The picture on the left highlights the Karman vortex sheets generated by droplets propagating in air.

4. Conclusions

The breaking of water waves induced by modulational instability has been numerically simulated by a two-fluid numerical approach. Simulations have been performed for two different values of the initial steepness and quantitative estimates of the energy transfer and momentum flux have been provided. The results show that in correspondence of the breaking events there is an energy transfer to the air, most of which is quickly by the viscous effects. It has been shown that the breaking occurrence enhances the mixing processes, and even without wind, the effects of the breaking arrive up to about one wavelength above the free surface. Further studies are needed in order to evaluate all the fluxes at the interface and to provide a more complete picture of the exchange phenomena at the interface, and thus a better understanding of the role of the breaking on the transfer processes occurring at the ocean-atmosphere interface.

Acknowledgements

The work has been financially supported by the "Flagship Project RITMARE - The Italian Research for the Sea - coordinated by the Italian National Research Council and funded by the Italian Ministry of Education, University and Research within the National Research Program 2014-2015". Authors express their gratitude to the Gerris team and Dr. S. Popinet not only for making the code available but also for the technical help provided (http://gfs.sourceforge.net). The numerical simulations of the Bejnamin-Feir instability have been done at CINECA, the Italian Supercomputing Center. We acknowledge the CINECA award under the ISCRA initiative, for the availability of high performance computing resources within the project IscrC_DIPWAVE. The technical support by Dr. Giorgio Amati is also gratefully appreciated.

References

[1] Janssen P 2009 The interaction of ocean waves and wind, Cambridge, UK, Cambridge Press
[2] Emmanuel K A 1986 An air-sea interaction theory for tropical cyclones. Part I: steady-state maintenance *J. Atm. Scien.* **43** 585-604
[3] Cavaleri L Fox-Kemper B and Hemer M 2012 Wind waves in the coupled climate system *Bull. Amer. Meteor. Soc.* **93** 1651-61

[4] Babanin A 2011 Breaking and dissipation of ocean surface waves Cambridge
[5] Deane G B and Stokes M D 1999 Air entrainment processes and bubble size distribution in the surf zone *J. Phys. Ocean.* **29** 1393-1403
[6] Kudryavtsev V N 2006 On the effects of sea drops on the atmospheric boundary layer *J. Geophy. Res.* **111**
[7] Cavaleri L 2009 Wave modelling – missing the peaks *J. Phys. Ocean.* **39** 2757-78
[8] Drazen D. and Melville W K 2009 Turbulence and mixing in unsteady breaking surface waves *J. Fluid Mech.* **628** 85-119
[9] Banner M L and Peirson W L 2007 Wave breaking onset and strength for two-dimensional deep-water wave group *J. Fluid Mech* **585** 93-115
[10] Iafrati A 2009 Numerical study of the effects of the beaking intensity on wave breaking flows *J. Fluid Mech.* **622** 371-411
[11] Iafrati A 2011 Energy dissipation mechanisms in wave breaking process: spilling and highly areated pluning breaking events *J. Geophy. Res.* **116**
[12] Tulin M P and Waseda T 1999 Laboratory observation of wave group evolution, includin breaking effects *J. Fluid Mech.* **378** 197-232
[13] Iafrati A, Babanin A and Onorato M 2014 Modeling of ocean-atmosphere interaction phenomena during the breaking of modulated wave trains *J. Copm. Phys.* **271** 151-71
[14] Benjamin T R and Feir J E 1967 The disintegratione of wave trains on deep water. Part 1. Theory *J. Fluid Mech.* **27** 471-30
[15] Popinet S 2009 An accourate adaptive solver for surface-tension-drive interfacial flows *J. Comp. Phys.* **228** 5838-66
[16] De Vita F, Verzicco R and A Iafrati 2015 Energy dissipation and spectrum evolution during the breaking of modulated wave trains *Proceeding of the 30th International Workshop Water Waves Floating Bodies,* Bristol, UK
[17] Lamont-Smith T, Fuchs J and Tulin M P 2003 Radat investigation of the structures of wind waves *J. Oceanogr.* **59** 49-63
[18] Landau L D and Lifshitz E M 1959 Fluid Mechanics *Pergamon Press*
[19] Iafrati A, Babanin A and Onorato M 2013 Modulational instability, wave breaking and formation of large-scale dipoles in atmosphere *Phy. Rev. Lett.* **110**
[20] Galchenko A, Babanin A, Chalikov D and Young L R 2010 Modulational instabilities and breaking strength for deep-water wave groups *J. Phys. Ocean.* **40** 2313-24
[21] Iafrati A and Campana E F 2005 Free-surface fluctuations behind microbreakers: space-time behaviour and subsurface flow field *J. Fluid Mech.* **529** 311-47